RSC ADVANCES

ARTICLE

Macroscopic Assembly of Flexible and Strong Green Graphene Fibres

R. Bakhtiari [a], S.Ghobadi [a], E. N. Güllüoğlu[b], L. I. Şanlı [c], S. A. Gürsel [a,c], E. Özden-Yenigün [b,d,*]

24Received 00th January 20xx,
Accepted 00th January 20xx

DOI: 10.1039/x0xx00000x

www.rsc.org/

Graphene fibres have great potential in future wearable electronics due to their promising thermal and electrical properties. However, fibre brittleness limits their implementation while the researchers are still seeking for easily scalable and eco-friendly production methods. Here we propose a green and continuous wet-spinning assembly approach to continuously spin flexible graphene oxide (GO) fibres. Highly stable aqueous GO suspensions up to 40 mg mL^{-1} are achieved and GO fibres are spun from highly oriented liquid crystals through customized continuous fibre production line. GO fibres with spesific ultimate tensile strength of 7 N/tex show strain to failure (%) of 10%; subsequent $NaBH_4$ chemical reduction gives graphene fibres with electrical conductivity of 214 S cm^{-1}. The scalable production presented here facilitates flexible strong and electrically conductive graphene fibres, which have emerged as promising graphene based electronic textiles and sensors.

Introduction

As a well-known two dimensional (2D) natural material, there have been numerous reports of graphene's superior electrical and mechanical characteristics, compared to other carbon nanomaterials [1, 2]. Graphene properties, empowered by its unique sp^2 formation of carbon atoms leading to 2D layered structures, have been desired in a variety of disciplines [3, 4]. These superior properties make graphene a perfect candidate in various fields including composites as reinforcement additives [5, 6], clean and renewable energy production [1-4] biocompatible thin films [1-7], nanoelectronics [8]. There have been several reports of different forms of graphene-based substances [5, 9]. Among which, the three-dimensional (3D) graphene fibres exhibit promising electrical, mechanical and thermal properties in macroscopic scale [10]. The previous studies have first led to formation of graphene oxide (GO) aqueous liquid crystals (GOLCs) for fibre spinning [9, 11-14]. The key of GOLCs preparation is to achieve the uniaxial alignment of GO layers called nematic phase [12], which is required for the optimum mechanical, electrical and morphological properties [15]. The substantial increase in alignment of GOLCs leads to better 3D macroscopic fibres as demanded both in academia and industry [9, 11-14, 16, 17] due to their high specific surface area and high tensile strength compared to other particle geometries [2, 18, 19]. The wet-spinning method, as a well-known approach for preparation of polyacrylonitrile based carbon fibres, possesses several advantages including easy scalability, low cost of operation, higher processing yield and eco-friendly manufacturing [20].There are several studies about the fabrication of graphene fibres however, to the best of our knowledge a very few of them offer continuous flexible green fibre production with the potential of scalability. For instance, Gao *et al.*, [11] prepared graphene fibres using wet-spinning method and the concentration of graphitic nanosheets used in the GOLCs was lower than 10 mg mL^{-1} whereas hydroiodic acid (HI) chemical reduction which prompts release of caustic by-product gases, was used. Besides, the low density of GO nanosheets in GOLCs and harsh reduction methods resulted in low layer packing inside the fibres, thus reduced their mechanical properties. In another study, Yu *et al.*, [21] produced pristine graphene fibres by a similar approach using surfactant coagulation bath. They observed better alignment of GO nanosheets in the GOLCs which leaded to higher packing density of graphene layers and better resultant properties. Not only GOLC characteristics but also the selection of coagulation media is an essential parameter which affects fibre tensile properties. As shown in **Table 1**, the GO fibres tensile strength coagulated in $CaCl_2$ bath is approximately three orders of magnitude higher than those prepared in different coagulation media such as CTAB, ethanol and NaOH [13, 21, 22]. In this approach, the elimination of functional groups present on the graphene layers are required to conduct electrons. Among different approaches such as thermal reduction [5], microwave irradiation [23], chemical reduction [24] method was the most reliable one without sacrificing the mechanical performance. At the same time, the defect density of graphene nanosheets is also tuneable compared to thermal reduction approach [11, 13, 25-27]

[a] *Faculty of Engineering and Natural Sciences, Sabanci University, 34956 Istanbul, Turkey*
[b] *Istanbul Technical University, Faculty of Textile Technologies and Design, Department of Textile Engineering, 34437, Istanbul, Turkey*
[c] *Nanotechnology Research and Application Center (SUNUM), Sabanci University, 34956 Istanbul, Turkey*
[d] *ITU Aerospace Research Center, Istanbul Technical University, Istanbul 34469, Turkey*
**Corresponding author:*ozdenyenigun@itu.edu.tr
Electronic Supplementary Information (ESI) available:
See DOI: 10.1039/x0xx00000x

RSC ADVANCES

ARTICLE

Table 1. Summarizes the studies conducted in literature by revealing process parameters and their final properties. (Hydroiodic acid (HI), cetyl trimethylammonium bromide (CTAB) and deionized water (DI))

Ref.	Coagulation Bath	Diameter (μm)	Reduction Method	Tensile Strength (GPa)	Conductivity (S m^{-1})
[10]	NaOH	40–150	HI (40 wt.%)	0.183	221
[11]	5 wt % NaOH / methanol	50–100	HI (40 wt.%)	0.14	2.5×10^4
[13]	Aqueous KOH;$CaCl_2$;$CuSO_4$	6	HI (30 wt.%)	0.36;0.5;0.48	3.9×10^4;4×10^4;3.8×10^4
[21]	Aqueous CTAB	60	HI (40 wt.%)	0.18	3.5×10^3
[22]	5 wt% NaOH ethanol	--	Hydrazine vapor	20.1	4.1×10^4
[26]	5 wt% NaOH ethanol	≈ 26	HI (40%)	0.19	2.3×10^4
[25]	Ethanol	10–60	HI (40 wt.%)	0.24	3.1×10^4
[28]	Glass pipeline	35	Thermal at 800 °C	0.42	10^3
[29]	Diethyl ether	50×10^4	Thermal at 1000°C	0.17	14×10^3

In this study, we aimed to propose scalable and green production of GO and graphene fibres without sacrificing mechanical and electrical properties. First, a mild process of GO synthesis based on Hummer's modified method was conducted while the temperature was reduced and via substitution of nitric acid with phosphoric acid production of NO_x pollutant gasses were eliminated[24, 30]. Afterwards, the GOLCs with dominant nematic phase formation were prepared via ultrasonic homogenization of GO nanosheets in aqueous media. At this stage, no surfactant and/or stabilizing agent was used to achieve 40 mg mL^{-1} GO concentration with densely packed GO nanosheets. Thus, pristine GO fibres were produced by avoiding the inevitable effect of surfactants and stabilizers on mechanism of electrical conduction. Then, GOLCs were wet-spun and for the first time systematically optimized fibre production line was designed for continuous, strong and electrically conducting graphene fibres. Various processing conditions (*e.g.* the feeding rate, take up speed and drawing speed) and coagulation composition were investigated and optimized through production (**Figure 1**). For fibre finishing, another systematic study on the improvement of electrical conductivity was conducted by exploring the effect of different chemical reduction methods. To the best of our knowledge, this study reports highest specific tensile strength for flexible and electrically conductive graphene-based single fibres, and also reveals the prerequisites of better mechanical, electrical and morphological properties by discussing the optimal material and process parameters. We should also emphasize that starting from GO synthesis to GO fibre reduction, green strategies including material and method selection has been promoted for flexible graphene fibre production.

Experimental Section

Graphene oxide (GO) synthesis via chemical oxidation

Graphite flakes (particle size +100 mesh (≥ 75% min) and melting point 3652-3697°C), potassium permanganate ($KMnO_4$), sulfuric acid (H_2SO_4), phosphoric acid (H_3PO_4), hydrogen peroxide (H_2O_2), hydrogen chloride (HCl), sodium borohydride ($NaBH_4$), HI, ascorbic acid (AA), calcium chloride ($CaCl_2$), sodium hydroxide (NaOH), and ethanol were purchased from Sigma-Aldrich and used without further purification. The improved synthesis protocol was tuned according to Hummer's method during which, $KMnO_4$ was mixed mechanically with natural graphite flakes. As a substantial change of nitric acid (HNO_3) in Hummers' modified method[24], H_3PO_4 was used in this study to have mild conditions[30] using the same protocol in ref [5]. First, one equivalent mass of graphite powder was put into glass flask placed in oil bath followed by pouring and mixing of $KMnO_4$ and graphite flakes with 6:1 mass ratio, respectively. Then, with respect to graphite flake mass fraction, 9:1 and 1:1 mass ratios

of H_2SO_4 and H_3PO_4, was added slowly to the initial solid mixture and distilled. The mixture was kept for 24 hours and then cooled by using ice bath. The resultant brownish slurry was introduced to the 20:1 (v:v) ice-H_2O_2 mixture for further neutralization. The final GO powder was washed with DI water and ethanol aqueous solutions several times. The GO nanosheets were dried for 48 hours at 70°C and conditioned.

GOLCs formation via high energy sonication

The chemical functionalization provides controlled exfoliation of graphite layers with hydrophilic functional groups [5]. Our functionalized GO can be readily dispersed in hydrous media with mild ultrasonic treatment due to the hydrogen bonding affinity of the existed surface functional groups. GOLCs were prepared in DI water at four different GO concentrations as 20, 25, 30 and 40 mg mL^{-1}. Each sample was sonicated during different consecutive periods (4 hours with cool-down intervals) in sonication bath (Power: 340 Watts) and later high power probe sonicated (Power: 650 Watts) as detailed in **Table S1**. At higher GO concentrations slightly higher energy was consumed. By eye examination, there is no changes observed at each GO concentration level due to tuned ultrasonication power.

Wet-spinning of GO fibres

Meter-scale continuous graphene fibres were produced by custom-designed wet-spinning line (**Figure 1**). For continuous production of neat GO fibres, the condensed aqueous GOLCs were injected through spinneret into the coagulation media at a rate of 60 µL min^{-1}. Based on previous studies, several chemicals (*e.g.* KOH, $CuSO_4$, NaOH, $CaCl_2$) were used for coagulation, however the best reported results were obtained at the coagulation baths of 5 wt.% and 3 wt.% NaOH in ethanol and $CaCl_2$ in 3:1 (v:v) ethanol: DI water solutions. The solidified GO fibre was collected onto the spinning drum at 70 rpm. The process was followed by washing with methanol to remove the residual coagulation chemicals. The collected fibres were dried for 24 hours at room temperature and conditioned. The wet-spinning process was conducted by the continuous spinning/washing custom setup **(Figure 1**) and **Table 2** gives the detailed fabrication parameters and the sample coding of produced GO fibres in our study. In this prototype spinning line as in industrial scale devices, the main factors such as flow rate, drawing speed through methanol washing with linear velocity 1.3 cm/sec and take up speed affecting the fibre properties were precisely controlled.

Chemical reduction of GO fibres

Three different reduction method were conducted as: (i) Reduction with HI aqueous solution 55 wt%, at 100°C [17], (ii) AA reduction, 2mM solution in DI water at 60°C [31] and (iii) ($NaBH_4$) [32] aqueous solution reduction. At this step, we explored the alternatives of harsh methods of hydrazine reduction and thermal reduction (See **Table 1**), so the proposed methodology could be easily implemented in large scale production. The reduced fibres were then washed with DI water for chemical removal and dried overnight at 60°C. A series of optimization studies was conducted based on the electrical conductivity of reduced fibres, by tuning time, temperature and concentration.

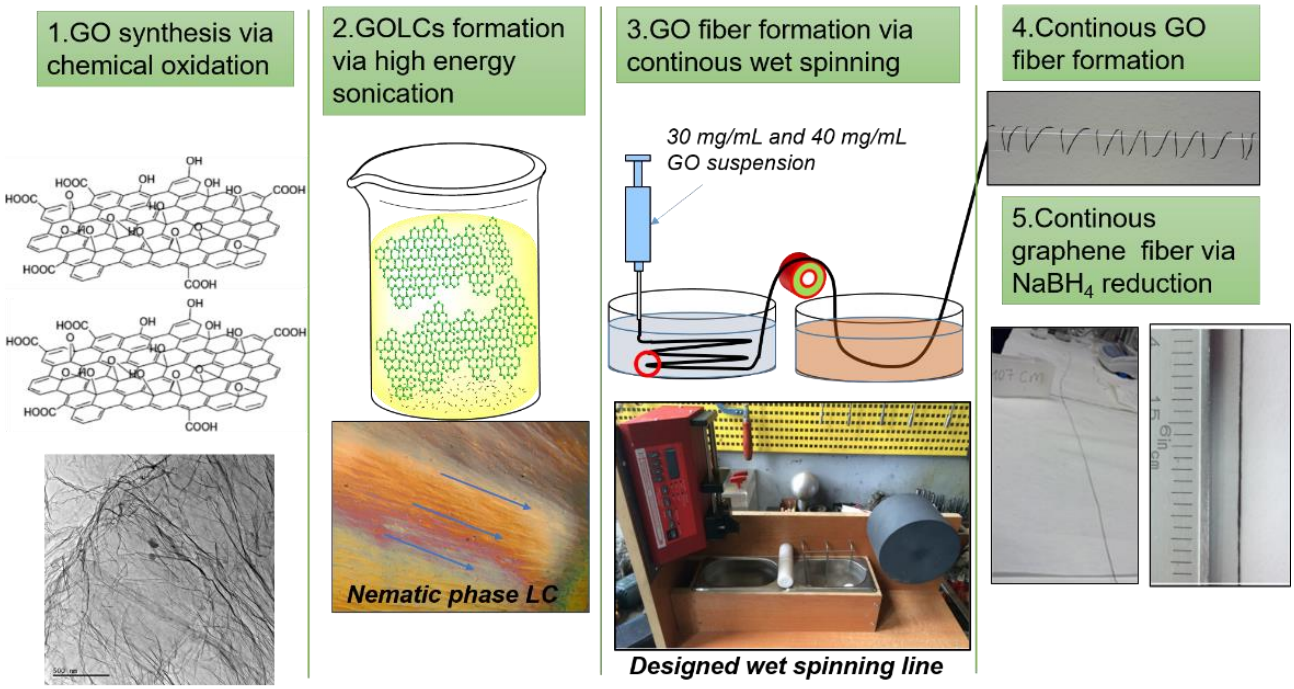

Figure 1. Schematic of continuous GO and electrically conducting graphene fibre formation via designed wet-spinning production line

RSC ADVANCES

ARTICLE

Table 2. GO concentration, coagulation bath composition and sample coding of as-spun GO fibre

GO Fibre	GO Concentration (mg mL^{-1})	Coagulation Bath Concentration (wt.%)	Coagulation Bath Composition
G20N3	20	NaOH (3)	Ethanol
G20N5	20	NaOH (5)	Ethanol
G20C3	20	$CaCl_2$ (3)	Ethanol: water(3:1)
G20C5	20	$CaCl_2$ (5)	Ethanol: water(3:1)
G25N3	25	NaOH (3)	Ethanol
G25N5	25	NaOH (5)	Ethanol
G25C3	25	$CaCl_2$ (3)	Ethanol: water(3:1)
G25C5	25	$CaCl_2$ (5)	Ethanol: water(3:1)
G30N3	30	NaOH (3)	Ethanol
G30N5	30	NaOH (5)	Ethanol
G30C3	30	$CaCl_2$ (3)	Ethanol: water(3:1)
G30C5	30	$CaCl_2$ (5)	Ethanol: water(3:1)
G40N3	40	NaOH (3)	Ethanol
G40N5	40	NaOH (5)	Ethanol
G40C3	40	$CaCl_2$ (3)	Ethanol: water(3:1)
G40C5	40	$CaCl_2$ (5)	Ethanol: water(3:1)

Characterization of GO nanosheets, GOLCs, GO fibres and graphene fibres

X-ray Diffraction (XRD) measurements of GO nanosheets, GO fibres and graphene fibres were performed with Bruker D-8 Advance X-Ray Diffractometer. The wavelength of irradiation of Cu K_α was 0.154 nm. The scan rate was 2.4°/min with the operating voltage of 40 kV and current of 40 mA. XRD measurements were carried out at 2Θ angle ranging from 5° to 90°. Raman spectroscopy investigations were conducted via Renishaw Raman spectrometer with a laser, excitation line at 532 nm, at spectral range of 100-3200 cm^{-1}. Polarized optical microscopy (POM) measurements of the GOLCs were conducted with a Carl Zeiss Axio Scope A1 MAT model POM in cross-polarized mode. For POM sample preparation, liquid nitrogen immersion for a few minutes in order to induce the GO layer packing for high quality imaging. To examine anisotropy of GOLCs, four different GOLCs concentrations as 20, 25, 30, 40 mg mL^{-1} were studied. Scanning electron microscope (SEM) images were performed on a field emission scanning electron microanalyzer (Zeiss LEO Supra 35 VP) at an acceleration voltage 5 kV in order to monitor the orientation and packing degree of GO fibres. Mechanical properties of the GO fibres were tested by Universal Testing Machine (UTM), Shimadzu AG-X plus with 1 kN load cell. The strain rate was 100 µm min^{-1} and testing speed was 0.5 mm min^{-1}. ASTM D3379-75 standard was followed. Test specimens were prepared, as shown in **Figure S1**, where the GO and graphene fibres were placed into frames with fixed 3 cm gauge length. At least 8 specimens were tested for each material set.

Electrical conductivity was conducted on the graphene fibres with a CR-Cascade Microtech CP 4-point probe conductivity measurement device. The probe distance was 1 mm. The electrical conductivity (σ) was calculated from the equation (1) [33] as:

$$\rho = \frac{(\frac{\pi t}{ln2})V}{i} = \frac{1}{\sigma} \qquad \text{(Equation 1)}$$

where ρ, t, V, and i are the resistivity, thickness, voltage, and current, respectively.

Results and Discussion

Structural Analysis of GO Nanosheets and Characterization of GOLCs

Figure 2a shows the XRD pattern of synthesized functionality rich GO nanosheets revealing two different 2Θ peaks of GO regarded as the proof for the presence of pendant groups and graphene layers. The sharp 2Θ peak at 9° pointed out the presence of graphene crystalline structure while the formation of pendant functional groups was confirmed by the broad 2Θ peak at 23°[11]. The rich functionalization of graphene layers through the chemical oxidation resulted in increased interlayer spacing of GO[11]. Nevertheless, addition of oxygen-containing groups intensified the defect density on the layered structure,

thus disturbing the ordered graphite layer packing. The presence of graphene layers also augmented intensity of 2Θ at 23° while the packing disturbance prompted through oxidation led to emergence of the 2Θ at 9° peak in the GO diffraction compared to graphite layer[5]. These two diffractions indicated that the oxidation of graphite layers was not only successful at the bulk but also its extent was enhanced towards the surface edges, where the presence of functionalities at that region was detected by the broad diffraction at around 2Θ=23°. The promoted oxidation for improved graphite layer exfoliation was in line with the observations of Xu *et. al* [13]. The intensity ratio of D and G peak (I_D/I_G) was calculated as 0.8 and 1.04 by integration for graphite and GO, respectively (**Figure 2b**). Compared to graphite, I_D/I_G of GO nanosheets reveals that the density of functional defects was higher in GO due to the increase in interlayer spacing [34] while graphite peak at 2750 cm^{-1} was completely removed from the GO spectrum. TEM micrograph of individual GO sheets (**Figure 2c**) showed that large, few-layers of GO can be obtained where physical perturbations were minimized. However, SEM micrograph (**Figure 2d**) revealed the multiple layer stacking in solid phase. Thus, one of the prerequisites to produce 3D structured GO fibres, is to have ordered GOLCs where the aligned GO nanosheets has been succeeded (**Figure 3**) [28].

The alignment of GOLCs was evaluated in cross-polarized mode POM. The birefringence behaviour of GOLCs assisted to the detection of distinctive domains visible by different contrasts (**Figure 3**), which pointed out the local alignment of GO layers in the liquid crystal phase. This local GO stacking reflected the *ordinary* and *extraordinary* rays of the polarized light by different angles, thus due to the cross-polarization of reflected light, local contrast differences were detected. To explore GOLC concentration effect on phase formations, first GOLCs at 20 and 25 mg mL^{-1} concentrations were studied. **Figure 3a** and **Figure 3b** revealed the nematic phase formation at these concentrations, whereas due to relatively short-range order of GO layers, the birefringence was quite limited. This effect was interpreted from the few numbers of birefringent sites with different contrasts in their respective POM images [10]. At 30 mg mL^{-1} GO concentration, more distinctive GOLC layer alignment leading multiple birefringence was observed (**Figure 3c**). The clear change in contrast and colour of nematic phase at higher concentrations was the result of their relatively different interference of ordinary and extraordinary light rays [35]. By varying the incident angle and so the interference of each locally aligned stacks, the colour contrast map changed and this enabled to visualize a series of local orientation sites in a single specimen [9]. **Figure 3d** displayed better alignment compared to lower concentrations so it is predicted that spinning at this concentration tends to form denser and stronger fibres due to long range order of GO layer stacks [10, 25].

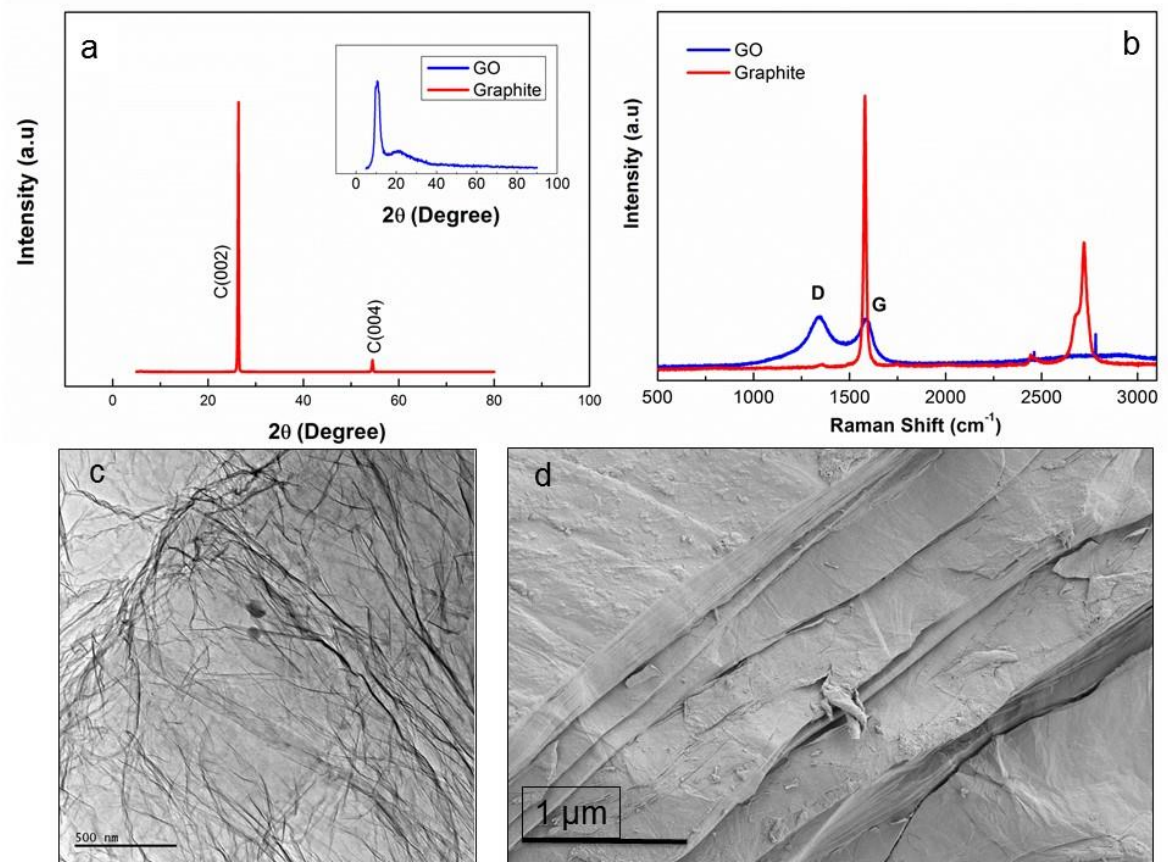

Figure 2. a) XRD analysis of graphite revealing (002) and (004) *hkl* planes and as inset image GO showing 2θ peaks of hydroxyl and carboxylic pendant groups at around 23° and graphene layers at 9°, b) Raman spectra of graphite (G and 2D peaks at 1550 and 2750 cm^{-1}) and GO (D peak at 1370 cm^{-1} and G peak at 1550 cm^{-1}), c) TEM and d) SEM micrographs of GO nanosheets

RSC ADVANCES

ARTICLE

Continuous GO fibre production via wet-spinning line

The continuous GO fibres were produced through a customized spinning line, where spinning and take-up speed were controlled effectively. A syringe pump to dispense GOLCs was used to control feeding rate. The spinneret designed with d/L>150 ratio was preferred to assist further alignment towards the flow direction for higher layer packing, ultimately for better fibre properties. Then, additional washing step was added to remove the coagulation bath residues by the aid of hydroxide groups in methanol. At this step, the residual NaOH and $CaCl_2$ moieties remained on fibres was also neutralized, thus improving the green nature of GO fibres. Besides, H_2O molecules interacted with GO was partially removed via dehydration of fibres, promoting an easier drying process. As an experimental point of view, the results showed that unwashed fibres had entrapped H_2O molecules even after three days while the methanol washed fibres were fully dry within a few minutes. Thus these dry fibres could be easily collected by a rotating drum without any noticeable damage.

The effect of coagulation media on structural and mechanical properties of fibres is still intriguing. Herein, we systematically studied the material parameters such as coagulation chemicals (*e.g.* $CaCl_2$, NaOH), their concentrations (*e.g.* 3 wt.%, 5 wt.%) and coagulation composition (*e.g.* ethanol, ethanol:water), as detailed in **Table 2**. Fibres coagulated in $CaCl_2$ coagulation bath (**Figure 4a- Figure 4d**) showed higher packing density compared to their equivalent GO fibres coagulated in NaOH (**Figure 4f** to **Figure 4h**). Nevertheless, we should emphasize that as in G40C5 and G40N5 fibres coagulated in NaOH (**Figure 4d** and **Figure 4h**), the packing density could be enhanced by increasing GO content. At such high GOLCs concentrations, the infusion of metal ions in coagulation bath could be prevented due to GO layer alignment and packing [28]. Thus, **Figure 4d** and **Figure 4h** exhibited similar packing densities free from coagulation medium. As expected, the surface topologies of low GO concentration fibres (*e.g.* 20 mg mL^{-1} and 25 mg mL^{-1}) were significantly different from high GO concentration fibres (*e.g.* 30 mg mL^{-1} and 40 mg mL^{-1}) in both coagulation media. The GO fibres produced from 20 mg mL^{-1} (**Figure 4a** and **Figure 4e**), and 25 mg mL^{-1} suspensions (**Figure 4b** and **Figure 4f**) had noticeable wrinkling effect and some irregular features. When GO concentration increased to 30 mg mL^{-1} (**Figure 4c** and **Figure 4g)** and 40 mg mL^{-1} (**Figure 4d** and **Figure 4h)**, such loose and irregular features were transformed to highly packed and extremely aligned structures. These densely packed fibres could withstand drawing and further finishing stresses during spinning, with showing higher tensile strength. Therefore, we observed that fibre formation was more successful even up to several meters at higher GOLCs concentration (*e.g.* 30 mg mL^{-1} and 40 mg mL^{-1}) (**Figure 1**). It is noteworthy that the reservoir capacity significantly affects the final fibre length in our spinning line and as predicted, larger reservoir leads to longer fibres[13, 29].

Mechanical Properties of GO fibres

GOLCs concentration, coagulation bath media and stress applied during spinning process has major effect on the final fibre properties. First, tensile properties of 40 mg mL^{-1} GO fibres (**Figure 5a**) and 30 mg mL^{-1} GO fibres (**Figure 5b**) coagulated in different media (detailed in **Table 2**) were compared. Each single fibre was implemented into UTM as shown in **Figure 5c**, where the cross-section of fibres might be varied due to their crumbled layered structures. Thus, as displayed in **Table 3**, specific ultimate strength (N/tex) was also calculated for each fibre class to eliminate fibre diameter effect due to the different ion diffusion mechanism in $CaCl_2$ and NaOH media. The results suggested that enhancement in the ultimate tensile strength of as-spun GO fibres due to higher GO concentration and GO stacking had minor effect about 10% depending on the coagulation medium, whereas strain to failure (%) decreased in general.

RSC ADVANCES

ARTICLE

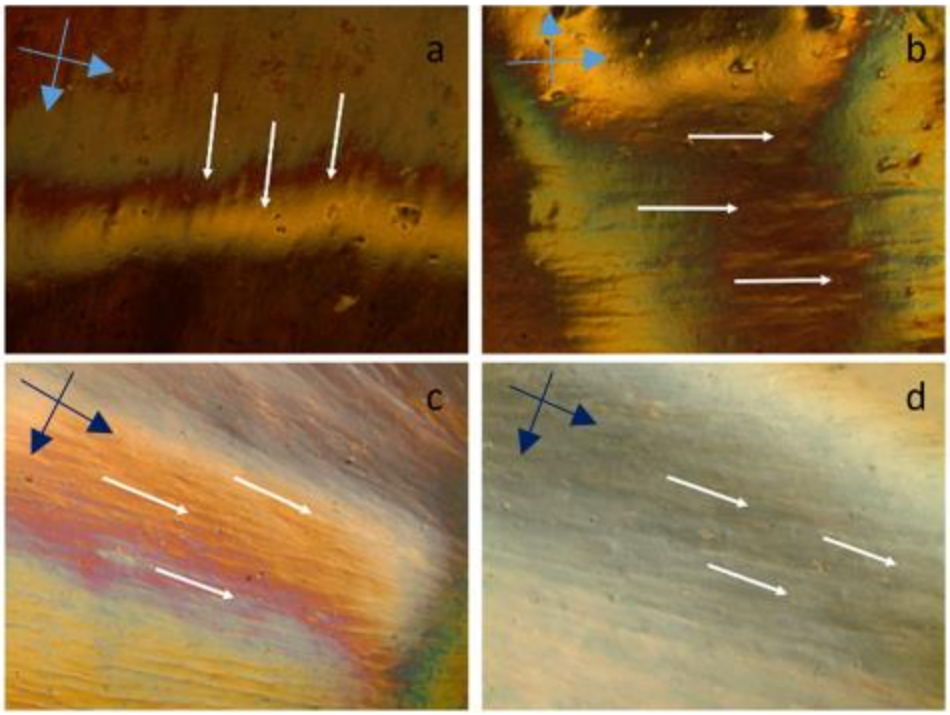

Figure 3. Cross polarized optical microscopy images of aqueous GOLCs at a) 20 mg mL^{-1}, b) 25 mg mL^{-1}, c) 30 mg mL^{-1} and d) 40 mg mL^{-1} GO concentrations. The cross dark arrows represent the cross-polarization direction.

Figure 5a pointed out that at same GO concentration level, the preference of $CaCl_2$ coagulation bath resulted in higher ultimate strength and strain to failure (%). For instance, G40C5 fibres coagulated in 5 wt.% $CaCl_2$ medium exhibited 2 fold higher ultimate strength and 5-fold increase in strain to failure compared to G40N5. Even though the same amount of GO dispensed, as shown in **Table 3**, mean fibre diameters differed drastically due to differences in ion diffusion mechanism. It is clear that $CaCl_2$ coagulation media which contains divalent Ca^{2+} ions, contributed to the fibre toughening and produced compact thinner fibres. The interaction between divalent metal ions (Ca^{2+}) and the carboxylic groups of the GO nanosheets has been explained by Park *et al*. [36]. They stated that divalent ions easily diffused into the fibre's interior, thus reacted completely with functional sites on the edges of GO sheets, which improved the toughness of the fibres [36]. Our results showed that not only ultimate strength but also strain to failure % was affected from these interactions. The affinity of Ca^{2+} ions towards GO sheets caused compact crumbled intrinsic morphologies and finally finer fibres. Higher number density of contact sites between each nanosheet induced much higher ultimate strain % and assisted plastic deformation mechanism. Meanwhile, the coagulation in NaOH media promoted in-situ partial reduction of GO layers, thus reducing the possibility of hydrogen bond network formation among the functional groups at the GO basal planes [12, 22]. It is noteworthy that GO concentration has minor effect on tensile properties [11, 37] while packing density and hydrogen bond network [26] promoted by coagulation process significantly dominate the mechanical response of fibres. **Figure 4i** and **Figure 5d** demonstrated the fracture surfaces of G30C5 and G40C5, respectively, where G40C5 fibres showed lower ductility than G30C5 fibres. Higher GO content per specific area contributed to brittleness of fibres due to the restrictions on plasticization. Restricted void formation and stress concentration sites might increase the strength while trading the ductility off. Overall, our results have shown that increasing GO content and packing density may alter fibre strength which would result in further changes in segmental mobility and depression of strain to failure (%).

As summarized in **Table 3**, compared to reference studies, proposed coagulation and washing protocol assembled more

flexible (about 9-fold) continuous GO fibres without impeding stiffness [26, 38].

Continuous graphene fibres via chemical reduction

Structural analysis of graphene fibres

The lack of electron conduction mechanism of as-spun GO fibres definitely limits the use of these fibres in sensing and electronic applications. To gain electrical conductivity, among several approaches chemical reduction was preferred due to possessing lower pollution and energy consumption [31, 32]. Besides, instead of using harsh reduction methods such as hydrazine and thermal treatment, we proposed an efficient green strategy to provide electrical conductivity. Thus, reduction process parameters including reaction time and temperature were also studied. Meanwhile these methods provide higher flexibility and versatility, and most importantly cause the reduction of graphene sheet disturbance (*e.g.* breakage and unintended layer dislocation) with promising mechanical properties of fibres [39]. Herein, flexible G30C5 fibres with the highest specific strength and larger ductility were selected for further chemical reduction studies. **Figure 6a** shows the suppression of functional groups presented in GO due to $NaBH_4$, AA and HI reduction, interpreted as decreased 2Θ at 9° in XRD spectra. Distinctively, 2Θ at 23° was completely removed only in $NaBH_4$ reduction process, revealing that proposed approach enabled the highest reduction degree in terms of interlayer spacing. Raman characterization of graphite and GO (**Figure 6b**) pointed out that the D peak at 1350 cm^{-1} was detected only for GO structure while the G peak, which indicates *E2g* mode of graphite layers, was seen at 1600 and 1650 cm^{-1} for graphite and GO, respectively [27]. The disruption of interlayer spacing leaded to G peak shifts in GO compared to graphite [40]. The D peak of Raman spectra of the graphene-based materials emerged in high intensity due to formation of structural defects within their layered formation of nanosheets[41]. The comparison between the I_D/I_G ratio of as-spun GO and reduced graphene fibres showed the level of success in elimination of functional group-driven defects, interpreted from reduced I_D/I_G ratio. **Figure 6b** suggests that $NaBH_4$ reduction approach (I_D/I_G=0.53) provided the most successful route to remove the structural defects.

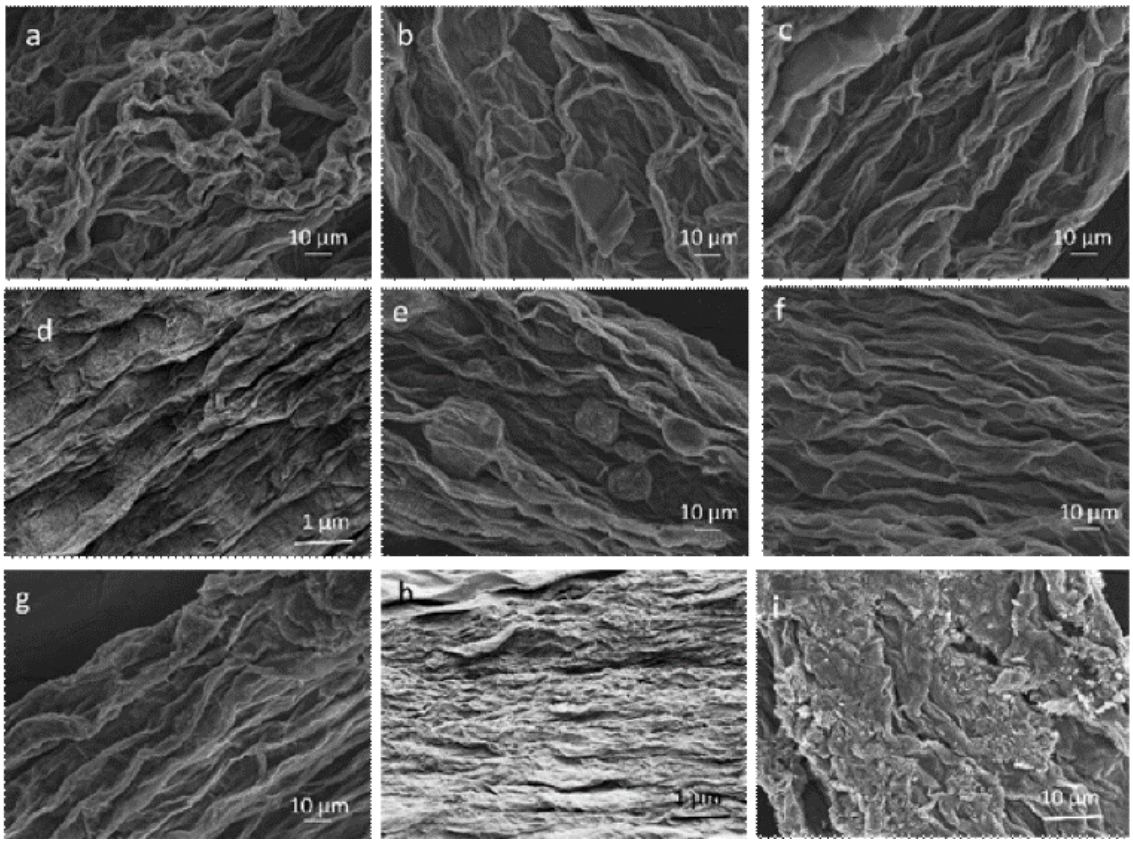

Figure 4. SEM images of a) G20C5, b) G25C5, c) G30C5, d) G40C5, e) G20N5, f) G25N5, g) G30N5, h) G40N5 coded GO fibres taken from their surfaces and i) fracture surface of G30C5 fibre after tensile testing

RSC ADVANCES

ARTICLE

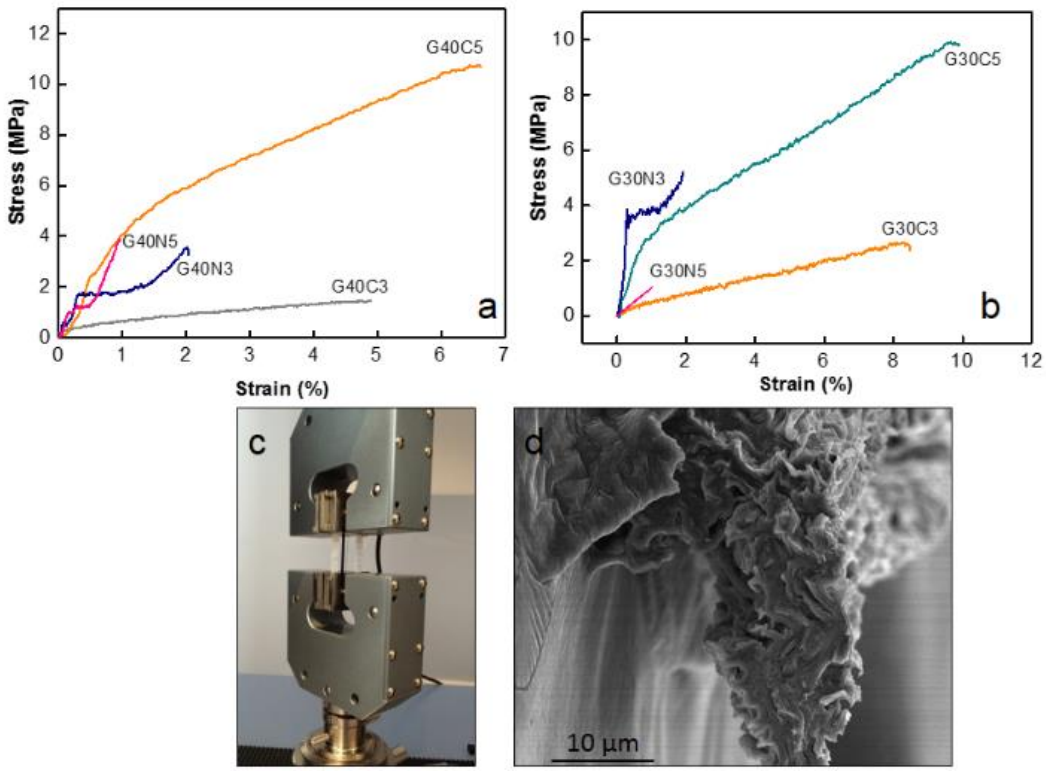

Figure 5. a) Stress(σ)-strain (ε) curve of 40 mg mL^{-1} GO coded fibres, b) Stress(σ) - strain (ε) curve of 30 mg mL^{-1} GO coded fibres, c) implementation of single GO fibre for tensile testing d) SEM image of the fracture surface of as-spun G40C5 fibre after testing revealing intrinsic crumbled structure

Table 3. Tensile properties of GO fibres coded in **Table 2** and reference studies from literature.

RSC ADVANCES

ARTICLE

GO Fibre	Diameter (μm)	Strain to failure (%)	Specific ultimate strength (N/tex)
G30C5	130	10±2.1	7±0.5
G40C5	130	6.7±0.5	5.9±1.3
reduced G30C5	229	4.7±0.5	4.5±2
reduced G40C5	271	2.8±1.7	14.5±0.4
G30N5	189	1.3±0.2	5.8±1.5
G40N5	203	0.9±0.1	6.4±0.7
GO fibre Ref[26] (draw ratio 1.09)	26	1.64±0.12	1.04±0.006
GO fibre Ref [26] (draw ratio 1.27)	26	0.84±0.08	1.26±0.013
Reduced GO fibre Ref [38]	240	1.5 ±0.1	1.02±0.03

Electrical conductivity of graphene fibres

We first attempt to reveal the effects of reducing agent and their relative reaction times on electrical conductivity of reduced fibres. It is assumed that 24 hours of reduction time enabled to reach stability for electrical conductivity [22]. However, **Figure 7a** unveiled that the highest electrical conductivity of 73 S cm^{-1} was achieved by $NaBH_4$ reduction after 72 hours. Hence, $NaBH_4$ reduction method was selected for further studies to explore temperature and concentration effect. The effect of temperature on electrical conductivity of $NaBH_4$ reduced fibres (**Figure 7b**) was investigated. Reduction kinetics at 90°C yielded 3 fold higher electrical conductivity compared to reduction at 30 and 60°C. Overall, $NaBH_4$ reduction at 90°C for 72 hours reached highest conductivity of 255 S cm^{-1}. Graphene fibres exhibited semiconductor characteristics as displayed in **Figure 7b**, as temperature increases, conductance increases resulting in dwindling of resistance. It could be associated to excitation of valence band electrons by temperature, as observed in semiconductors.

In shorten reaction times at 90°C, we enquired into $NaBH_4$ concentration (from 0.3M to 2.4 M) effect. **Figure 7c** revealed the highest electrical conductivity of 214 S cm^{-1} along fibre axis prevailed at concentration of 2.4 M $NaBH_4$. The high conductivity of graphene fibres is believed to be due to increased number of reduced sites. This effect further leads to higher conductivity of reduced graphene fibres while preserving the oriented fibre structure which minimized the contact resistance. The combination of good flexibility, high tensile strength and enhanced electrical conductivities of graphene fibres make stretchable wires for promising wearable functional textiles. Thus, G30C5 and G40C5 GO fibres reduced by eco-friendly $NaBH_4$ (2.4 M) at 90°C for 24 hours were tested under tensile loading, in next section.

RSC ADVANCES

ARTICLE

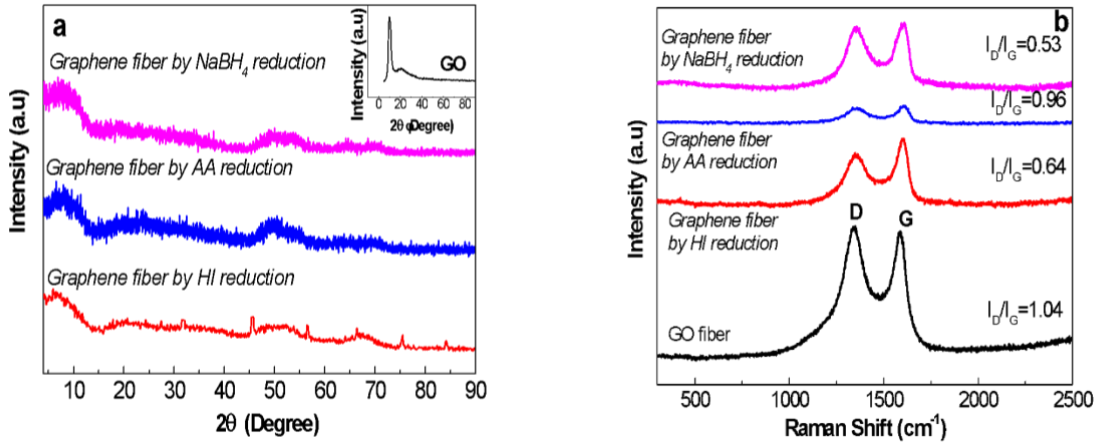

Figure 6. a) XRD spectra (the inset figure represents the XRD spectrum of GO sheets as detailed in Figure 2) and b) Raman spectra of GO and graphene fibres reduced by $NaBH_4$, AA and HI agents revealing D peak at 1370 cm^{-1} and G peak at 1550 cm^{-1}.

Mechanical properties of graphene fibres

To calculate the mechanical behaviour of graphene fibres and monitor the effect of reduction process, we performed tensile testing of both reduced G30C5 and G40C5 fibres. The mechanical tests described in experimental section were carried out to determine the stress-strain behaviour along fibre direction (**Figure 8**). **Table 3** also summarizes ultimate tensile strength and strain to failure (%) of G30C5 and G40C5 graphene fibres. Here, we first investigate the change in strain to failure (%) during the process of reduction. $NaBH_4$ reduction caused swollen fibres, which failed in brittle manner. This change in ductility could be associated to prevented slipping of graphene layers due to the corrupted network after reduction. Furthermore, depending on GO density, ultimate specific strength might be increased or decreased [27]. For instance, tensile ultimate strength drastically improved for reduced G40C5 graphene fibres, whereas there is slight reduction observed in reduced G30C5 graphene fibres. Apart from the spinning process, the structural difference of these fibres came from the presence of higher number of reduction sites. The graphene fibres with higher degree of reduction as in G40C5 fibres were less affected from this post process in terms of tensile strength whereas high number of stiff graphene sheets prevented plastic deformation and caused brittle failure. We should also note that the specific stress of reduced G30C5 graphene fibres was higher compared previous studies as described in **Table 3**.

RSC ADVANCES

ARTICLE

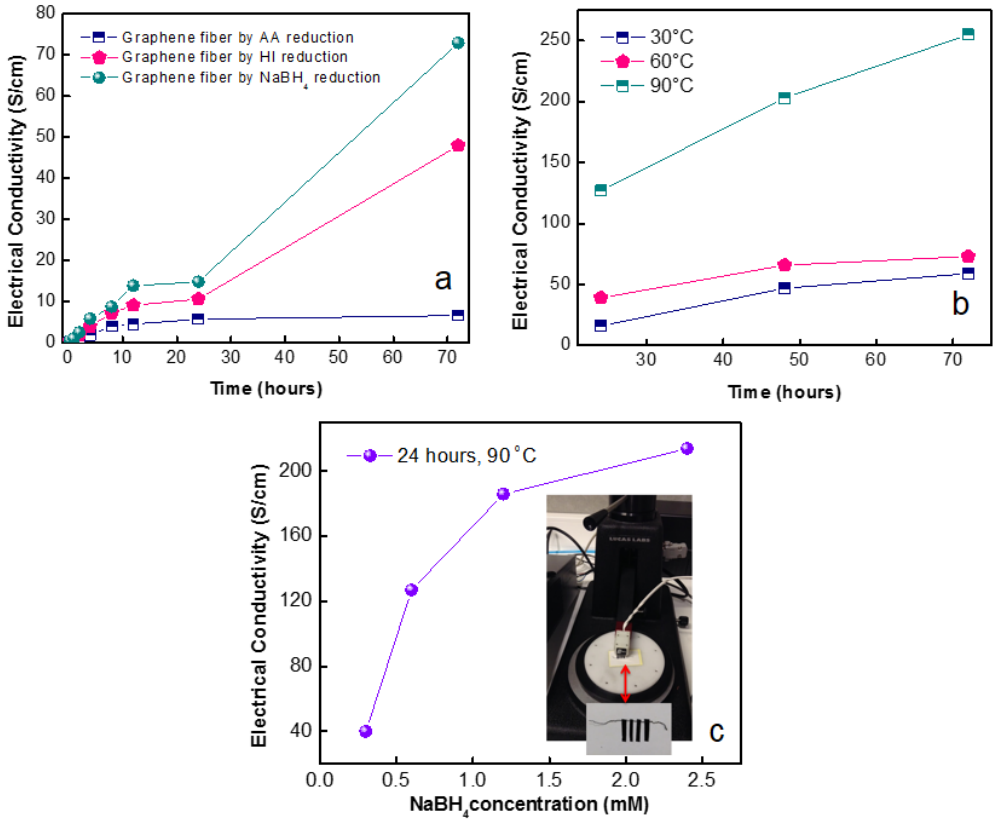

Figure 7. Electrical conductivity of graphene fibres by revealing a) effect of reducing agent depending on reaction time, b) effect of reduction times depending on temperature for $NaBH_4$ (1.2 M) reducing agent, c) effect of $NaBH_4$ concentration

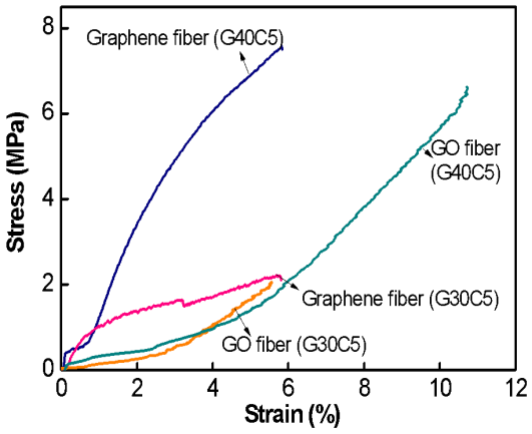

Figure 8. Stress (σ)-strain (ε) curves of G30C5, G40C5 GO fibres and reduced G30C5 and G40C5 graphene fibres

RSC ADVANCES

ARTICLE

Conclusion

Scalable production of graphene oxide and graphene fibres from stable aqueous GOLCs were fabricated via the designed continuous wet-spinning line while process (*e.g.* the feeding rate, take up speed and drawing speed) and material parameters including coagulation composition and concentration were precisely controlled through the proposed green approach. The results show that as-spun GO fibres coagulated in $CaCl_2$ ensured promising tensile properties where reduced GO fibres showed strain to failure (%) of 10% with higher specific ultimate strength. $NaBH_4$ reduction approach (I_D/I_G=0.53) performed at 90°C for 24 hours with 2.4 M concentration, enabled facile route to gain electrical conductivity while individual reduced G30C5 fibres exhibited electrical conductivity of 214 S cm^{-1} along fibre axis. Overall we suggest that green and scalable production of graphene fibres could have promising applications in sensing and wearable electronics since they are non-toxic, flexible and have high tensile strength.

Acknowledgements

This research has received funding from the Scientific and Technological Research Council of Turkey (TUBITAK) under project number 214M398.The authors thank to MSc student Ismail Kaya for his help in wet spinning set up.

References

1. L. Işıkel Şanlı, V. Bayram, B. Yarar, S. Ghobadi and S. Alkan Gürsel, *International Journal of Hydrogen Energy*, 2016, **41**, 3414-3427.
2. F. Lin, X. Tong, Y. Wang, J. Bao and Z. M. Wang, *Nanoscale Res Lett*, 2015, **10**, 435.
3. L. Işıkel Şanlı, V. Bayram, S. Ghobadi, N. Düzen and S. Alkan Gürsel, *International Journal of Hydrogen Energy*, 2017, **42**, 1085-1092.
4. H.-P. Cong, J.-F. Chen and S.-H. Yu, *Chemical Society Reviews*, 2014, **43**, 7239-7456.
5. S. Ghobadi, S. Sadighikia, M. Papila, F. Ç. Cebeci and S. A. Gürsel, *RSC Advances*, 2015, **5**, 85009-85018.
6. S. Ghobadi, S. Mehraeen, R. Bakhtiari, B. Shamloo, V. Sadhu, M. Papila, F. Ç. Cebeci and S. A. Gürsel, *RSC Advances*, 2016, **6**, 92434-92442.
7. J. Li, G. Wang, H. Zhu, M. Zhang, X. Zheng, Z. Di, X. Liu and X. Wang, *Scientific reports*, 2014, **4**, 4359.
8. T. Mosciatti, S. Haar, F. Liscio, A. Ciesielski, E. Orgiu and P. Samorı`, *American Chemical Society*, 2015, **9**, 2357-2367.
9. Z. Xu and C. Gao, *Accounts of chemical research*, 2014, **47**, 1267-1276.
10. R. Jalili, S. H. Aboutalebi, D. Esrafilzadeh, R. L. Shepherd, J. Chen, S. Aminorroaya-Yamini, K. Konstantinov, A. I. Minett, J. M. Razal and G. G. Wallace, *Advanced Functional Materials*, 2013, **23**, 5345-5354.
11. Z. Xu and C. Gao, *Nature communications*, 2011, **2**, 571.
12. P. Kumar, U. N. Maiti, K. E. Lee and S. O. Kim, *Carbon*, 2014, **80**, 453-661.
13. Z. Xu, H. Sun, X. Zhao and C. Gao, *Adv Mater*, 2013, **25**, 188-193.
14. Z. Liu, Z. Li, Z. Xu, Z. Xia, X. Hu, L. Kou, L. Peng, Y. Wei and C. Gao, *Chemistry of Materials*, 2014, **26**, 6786-6795.
15. X. Yang, C. Guo, L. Ji, Y. Li and Y. Tu, *Langmuir : the ACS journal of surfaces and colloids*, 2013, **29**, 8103-8107.
16. K. E. Lee, J. J. Oh, T. Yun and S. O. Kim, *Journal of Solid State Chemistry*, 2015, **224**, 115-119.
17. Z. Tian, C. Xu, J. Li, G. Zhu, Z. Shi and Y. Lin, *ACS applied materials & interfaces*, 2013, **5**, 1489-1493.
18. B. Dan, N. Behabtu, A. Martinez, J. S. Evans, D. V. Kosynkin, J. M. Tour, M. Pasquali and I. I. Smalyukh, *Soft Matter*, 2011, **7**, 11154-11159.
19. N. Behabtu, J. R. Lomeda, M. J. Green, A. Sinitskii, D. V. Kosynkin, J. Schmidt, E. Kesselman, M. Pasquali, A. L. Higginbotham, D. Tsentalovich, Y. Talmon, A. N. G. Parra-Vasquez, J. M. Tour and Y. Cohen, *Nature Nanotechnology*, 2010, **5**, 406-411.
20. A. H. Wazir and L. Kakakhel, *New Carbon Materials*, 2009, **24**, 83-88.
21. H. P. Cong, X. C. Ren, P. Wang and S. H. Yu, *Scientific reports*, 2012, **2**, 613.
22. L. Chen, Y. He, S. Chai, H. Qiang, F. Chen and Q. Fu, *Nanoscale*, 2013, **5**, 5809-5815.
23. W. Chen, L. Yan and P. R. Bangal, *Carbon*, 2010, **48**, 1146-1152.
24. D. C. Marcano, D. V. Kosynkin, J. M. Berlin, A. Sinitskii, Z. Sun, A. Slesarev, L. B. Alemany, W. Lu and T. J. M., *ACS Nano*, 2010, **4**, 4806-4814.
25. G. Huang, C. Hou, Y. Shao, H. Wang, Q. Zhang, Y. Li and M. Zhu, *Scientific reports*, 2014, **4**, 4248.
26. C. Xiang, C. C. Young, X. Wang, Z. Yan, C. C. Hwang, G. Cerioti, J. Lin, J. Kono, M. Pasquali and J. M. Tour, *Adv Mater*, 2013, **25**, 4592-4597.
27. S. Hussain, C. Yorucu, I. Ahmed, R. Hussain, B. Chen, M. Bilal Khan, N. A. Siddique and I. U. Rehman, *Surface and Coatings Technology*, 2014, **258**, 458-466.
28. Z. Dong, C. Jiang, H. Cheng, Y. Zhao, G. Shi, L. Jiang and L. Qu, *Adv Mater*, 2012, **24**, 1856-1861.
29. S. Zhang, K. K. Koziol, I. A. Kinloch and A. H. Windle, *Small*, 2008, **4**, 1217-1222.
30. J. W. S. Hummers and R. E. Offeman, *Journal of American Chemical Society*, 1958, **80**, 1339.
31. M. J. Ferna´ndez-Merino, J. I. P. L. Guardia, S. Villar-Rodil, P. Soli´s-Ferna´ndez, A. Marti´nez-Alonso and J. M. D.

Tasco´n, *Journal of Physical Chemistry C*, 2010, **114**, 6426-6432.
32. H.-J. Shin, K. K. Kim, A. Benayad, S.-M. Yoon, H. K. Park, I.-S. Jung, M. H. Jin, H.-K. Jeong, J. M. Kim, J.-Y. Choi and Y. H. Lee, *Advanced Functional Materials*, 2009, **19**, 1987-1992.
33. D. S. McLachlan, *Journal of Physics C: Solid State Physics*, 1985, **18**, 1891-1897.
34. F. T. Thema, M. J. Moloto, E. D. Dikio, N. N. Nyangiwe, L. Kotsedi, M. Maaza and M. Khenfouch, *Journal of Chemistry*, 2013, **2013**, 6.
35. R. Niu, J. Gong, D. Xu, T. Tang and Z.-Y. Sun, *Colloids and Surfaces A: Physicochemical and Engineering Aspects*, 2015, **470**, 22-30.
36. S. Park, K.-S. Lee, G. Bozoklu, W. Cai, S. T. Nguyen and R. S. Ruoff, *ACS Nano*, 2008, **2**, 572-578.
37. Z. Dong, C. Jiang, H. Cheng, Y. Zhao, G. Shi, L. Jiang and L. Qu, *Adv. Mater.*, 2012, **24**, 1856-1861.
38. S. Chen, W. Ma, Y. Cheng, Z. Weng, B. Sun, L. Wang, W. Chen, F. Li, M. Zhu and H. M. Cheng, *Nano Energy*, 2015, **15**, 642-653.
39. S. Pei, J. Zhao, J. Du, W. Ren and H.-M. Cheng, *Carbon*, 2010, **48**, 4466-4474.
40. L. I. Şanlı, V. Bayram, B. Yarar, S. Ghobadi and S. A. Gürsel, *Int. J. Hydrogen Energy*, 2016, **41**, 3414-3427.
41. S. Stankovich, D. A. Dikin, R. D. Piner, K. A. Kohlhaas, A. Kleinhammes, Y. Jia, Y. Wu, S. T. Nguyen and R. S. Ruoff, *Carbon*, 2007, **45**, 1558-1565.